EFFECTS OF FIBRE ARCHITECTURE ON DEFORMATION DURING PREFORM MANUFACTURE

A.C. Long, B.J. Souter, F. Robitaille, and C.D. Rudd

School of Mechanical, Materials, Manufacturing Engineering & Management,
Division of Mechanical Engineering, University of Nottingham,
University Park, Nottingham NG7 2RD, UK

SUMMARY: Simulations of fabric deformation during preform manufacture are usually based on a kinematic mapping of the fibres onto the component. Whilst this approach can anticipate excessive deformation, it takes no account of the effect of fabric construction on subsequent forming characteristics. The aim of this study is to establish a relationship between fibre architecture and formability, and to incorporate this within an enhanced draping simulation. The approach utilises a geometric model for woven or warp-knitted fabrics, which forms the basis of a mechanical model for fabric deformation. The model is then used to determine the shear strain energy required to produce a particular draped fibre pattern. This is implemented within an iterative procedure to determine the draped pattern resulting in minimum strain energy. The results compare favourably with experiments for hemispherical preforms, where initial fabric construction is shown to have a significant effect on the resulting fibre orientations.

KEYWORDS: textile preforms, fabric shear, drape modelling, liquid composite moulding

INTRODUCTION

Preforms for use in liquid moulding processes can be produced via forming or draping of reinforcement fabrics. Reinforcements are available in a number of forms, including woven and warp-knitted (stitch-bonded) fabric structures. There are now a large number of suppliers, each providing a range of fabrics with different characteristics. Materials selection, therefore, can be a difficult and time-consuming process if based on trial and error. Over the last ten years, a number of studies have been carried out into fabric deformation characteristics and deformation modelling. This has led to the development of test methods for fabric formability, usually based on either simple shearing or uniaxial extension along the bias [1-3]. Over a similar period, a number of fabric deformation models or drape simulations have been developed [eg. 4,5]. These simulations are usually based on a kinematic mapping of the fibres onto the surface of the preforming tool, and can be used to anticipate changes in fibre

orientations and volume fractions, from which subsequent properties such as permeability and elastic constants may be inferred.

Although a number of fabric drape simulations are now available, the majority of these make no attempt to account for the differences between fabrics, other than in the specification of a "locking angle" which indicates the limit of deformation. Indeed the above mentioned work on characterisation of fabric deformation has, for the most part, taken place in isolation from the development of deformation simulations. The authors have shown that fabric construction can have a significant effect on the deformed fibre pattern, even for simple shapes such as hemispheres or disks [2]. This is particularly evident for warp-knitted fabrics, where shear forces and subsequent fabric locking angles can differ for deformation parallel and perpendicular to the stitching thread. Some potential for inclusion of fabric specific effects has been shown in the development of finite element simulations for fabric/composite forming [eg. 6,7], but these possibilities have not been explored to date.

The objectives of this study were to investigate the possibility of incorporating aspects of fabric deformation mechanics within an existing drape simulation. The intended approach is to use the traditional pin-jointed approximation within an iterative scheme based on minimization of shear strain energy. The first stage in this process was to develop a geometric model for fabric reinforcements, which could be used as a basis for a mechanical model of fabric shear. Results from the shear model can be used to generate shear strain energy data, which can be incorporated within the iterative drape simulation. This is demonstrated for two warp-knitted fabrics, which illustrate the effects of initial fibre architecture on the subsequent deformed fibre pattern.

FABRIC GEOMETRIC MODEL

Before a general model for the mechanics of fabric deformation can be developed, it is first necessary to develop a model to describe the initial fibre architecture. This description can also be used as a basis for the prediction of subsequent flow properties (permeability). In this section, a single definition is proposed for the interlacing patterns of woven and warp-knitted fabrics. The definition consists of a series of vectors which describe the paths of individual tows between crossover or intersection points. Although the basis of the definition is general, additional specifications are required for woven fabrics (to define the weave pattern) and warp-knitted fabrics (to define the stitching pattern).

Woven Fabrics

To describe the interlacing pattern for a woven material, it is first necessary to specify the number of levels on which the warp-wise ($L_{i,wp}$) and weft-wise ($L_{i,wt}$) tows are positioned (Fig. 1). A standard fabric features one level in both the warp and the weft directions, whereas entering a total number of levels greater than two creates a 3D woven textile. The levels are identified sequentially (L_i), firstly for warp-wise tows and then for weft-wise tows. The dimensions of the repeating cell are then specified by defining the number of warp-wise (RC_{iwp}) and weft-wise (RC_{iwt}) tows present in the unit cell along with the tow spacings. Following this, the tow type is specified for warp-wise and weft-wise tows at each level in the repeating cell. This allows fabrics to be represented which include more than one tow type (for example, a hybrid carbon/glass fabric or a quasi-unidirectional material with a light transverse tow). Each crossover in the repeating cell is defined within the weaving matrix

[$\mathbf{WP_i}$] of dimensions $RC_{i.wp}$, $RC_{i,wt}$. The interlacing pattern of the reinforcement is defined by entering the level identifiers (L_i) of each tow from bottom to top for each crossover into this matrix (Fig. 2).

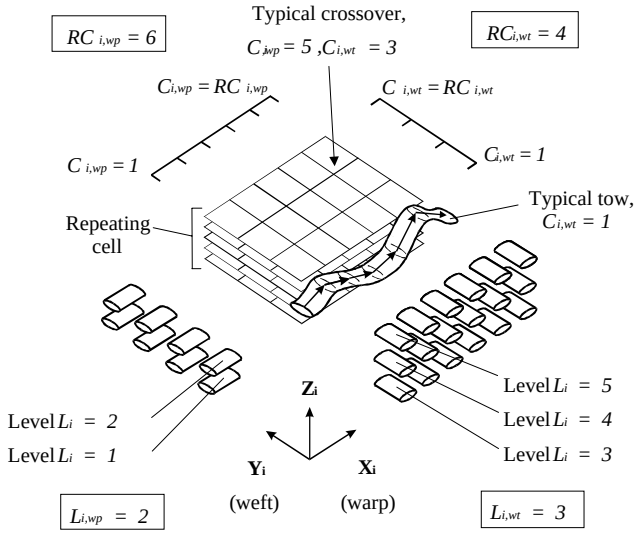

Fig. 1: Interlacing patterns for woven materials.

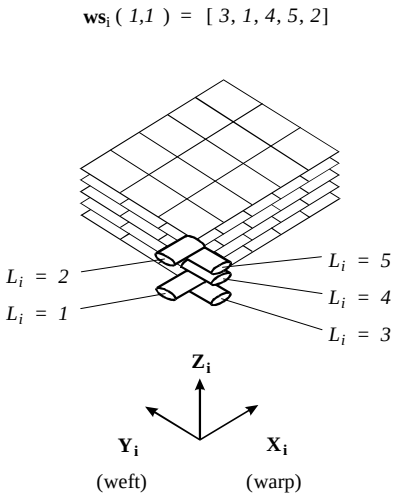

Fig. 2: Vectorial term $\mathbf{ws_i}$ (1 , 1), defining the interlacing sequence.

The quantities defined above allow vectors defining the interlacing pattern to be generated over the repeating cell by rearranging the weaving matrix [$\mathbf{WP_i}$] and combining with the values of the tow spacing. Whereas the vectors define the correct in-plane dimensions, the out-of-plane dimension (ie. fabric thickness) is defined as an integer. This is because it is difficult to obtain an accurate measure of the tow thickness. Ultimately the intention is to predict this with a mechanical model for tow deformation.

Warp-Knitted Fabrics

Warp-knitted (stitch-bonded or non-crimp) fabrics consist of reinforcement tows held together by stitching threads. To specify the interlacing patterns for these textiles, the user first specifies the number of non-interlacing levels of tows ($L_{i,tow}$), and the number of levels of warp-knitted threads ($L_{i,thread}$) as shown in Fig. 3. Individual levels are given a unique number for both the non-interlaced tows ($L_{i,w}$) and the warp-knitted threads ($L_{i,d}$).

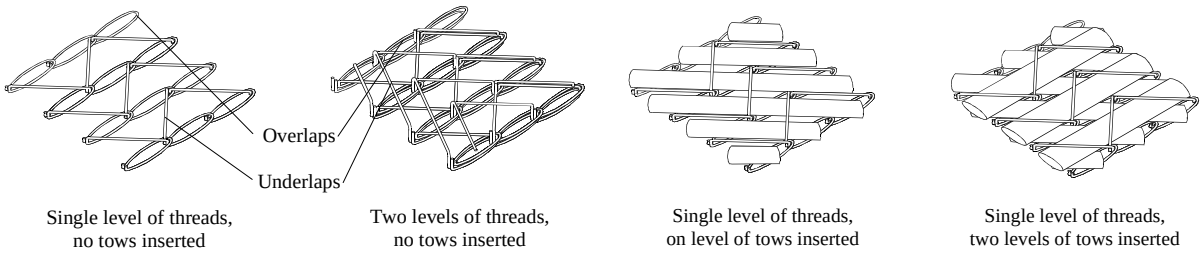

Fig. 3: Warp-knitted textiles: $L_{i,thread}$ levels of threads assembled by $L_{i,tow}$ levels of tows.

During the warp-knitting process, the threads are looped around $N_{i,needle}$ needles using a guide bar, to form a continuous stitch consisting of overlaps (loops) and underlaps (straight segments). The positions of the overlaps and underlaps are easily traced on a warp-knitted textile and can be mapped onto a grid, allowing the knitting sequence to be determined. This sequence corresponds to the "chain" used on industrial warp-knitting machines (Fig. 4). Due to the nature of the process, all threads formed on each level $L_{i,d}$ follow the same pattern. Underlaps and overlaps from different levels of threads $L_{i,d}$, knitted by different guide bars, never interlace among or between themselves.

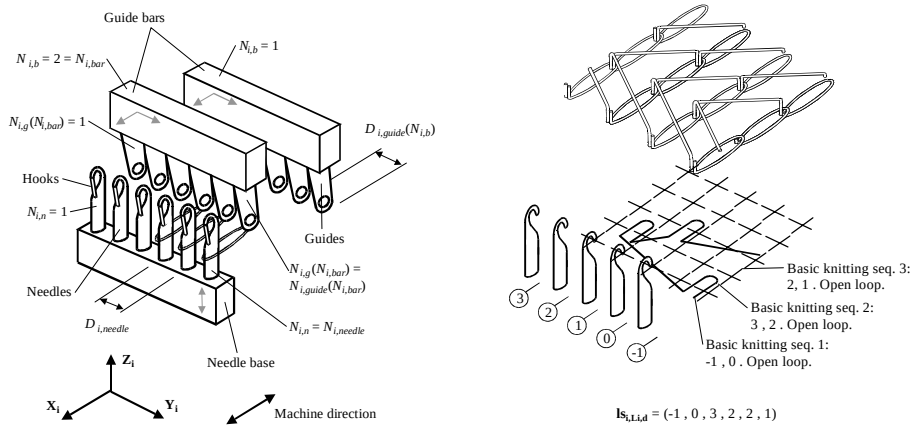

Fig. 4: Configuration of a warp-knitting machine and lapping sequence.

The knitting sequence is specified ($\mathbf{ls_{i,Li,d}}$) for threads at each level $L_{i,d}$. Each integer in the knitting sequence corresponds to a gap between the needles of the warp-knitting machine (Fig. 4). The length of the overlaps, the distance $D_{i,needle}$ between adjacent needles, and the number of empty thread guides present between two loaded guides (if any) are then defined. The tow orientations are specified for each level of tows. As for the description of woven textiles, the types of the tows are also specified.

Reinforcement tows can be inserted between the overlaps and the underlaps, or between the underlaps of any two adjacent levels of threads. The interlacing pattern of the tows and threads can also be varied over the surface of the textile. This capability allows the representation of most commercial warp-knitted textiles. Consequently, the interlacing pattern is specified for each warp-knitted unit cell, as a matrix containing the level number $L_{i,d}$ of the first underlap found above each tow, in sequence. From these expressions the vectors that represent the repeating cell of the warp-knitted textile can be generated. The expressions developed for the description of warp-knitted textiles also allow self-checks to be performed for the structure generated (eg. to ensure that all tows are integrated).

Demonstration of Geometric Model

Before the geometric description of a fabric can be used for mechanical analysis, the description needs to be verified to ensure that it provides an accurate representation. In order for this to be done, a viewing program has been developed allowing the user to enter, check and save a fabric description. Fig. 5 shows typical outputs from this program, where the user has entered the fabric description for a four-harness satin weave and a 0-90° warp-knitted fabric with a tricot 1 and 1 stitch.

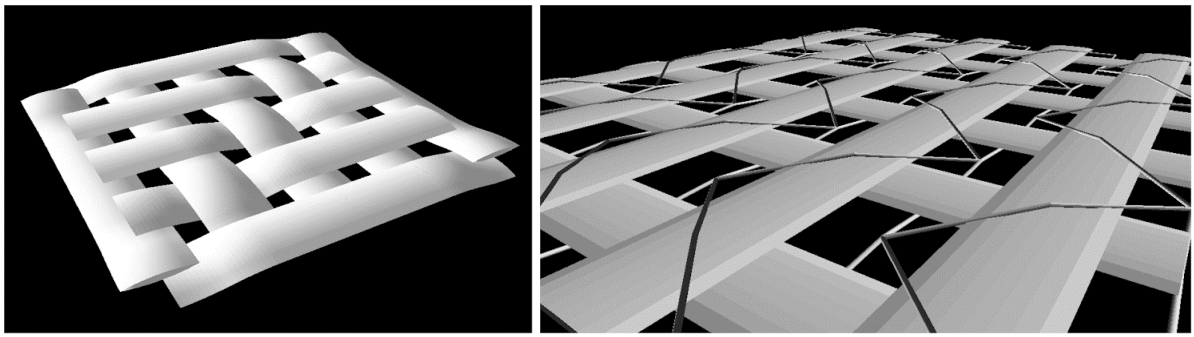

Fig. 5: Graphical representations of fabric geometric model – four-harness satin weave (left) and 0/90° tricot stitched fabric (right).

MECHANICAL MODEL FOR FABRIC SHEAR

To determine the effects of fibre architecture on fabric formability, a mechanical model for fabric deformation is under development. This will utilise the information provided by the fabric geometric model to determine the shear force and ultimately the limit of deformation for an arbitrary textile structure. This has been implemented for in-plane shearing of a plain weave fabric, as described below. It is intended that a similar approach will be adopted for other fibre architectures, although it is recognised that an alternative model may be required for warp-knitted textiles to account for the tensile properties of the stitching thread.

For a general woven textile, three deformation modes are considered: tow flexion, inter-tow rotational friction at the crossovers, and tow compaction. These three modes essentially occur in a sequential manner as in-plane shear deformation is imposed. A series of assumptions were used in the development of the model for plain weaves:

- Tow paths are lenticular;
- Even contact is achieved at tow crossovers;
- Tow width (T_w) varies during shearing, whereas tow spacing (T_s) is constant;
- Fabric thickness remains constant during shearing.

Many geometrical descriptions of a plain-weave unit cell have been proposed, including circular, sinusoidal and elliptical tow cross-sections or paths. However experimental observations support the assumption of a lenticular path. The assumption of constant fabric thickness during shearing is based on experimental measurements by McBride [3].

As observed by Kawabata [8], after an initial (often negligible) contribution from the tow flexural rigidity, the main resistance to deformation comes from the friction at tow crossovers. Neglecting the flexural rigidity, the shear force can be obtained by considering torque at each crossover:

$$T_r = \mu_{cr} \times F_c \times R_{eff} \tag{1}$$

where μ_{cr} is the coefficient of friction at the crossover (assumed to be 0.3), and F_c is the contact force. R_{eff} is the effective radius of rotation through which the torque acts:

$$R_{eff} = \frac{1}{A}\int_A r dA \tag{2}$$

where A is the tow contact area, which is assumed to be a parallelogram formed by the outlines of the contacting tows. Calculation of the effective radius relies on accurately predicting the tow width. From simple geometric considerations, the tow width would be expected to obey the following relationship with shear angle, θ:

$$\begin{aligned} T_w &= T_{w0} && \theta \le \theta_{Li} \\ T_w &= T_s \cdot \cos(\theta) && \theta > \theta_{Li} \end{aligned} \tag{3}$$

where T_{w0} is the initial tow width, and the angle at which adjacent tows come into contact is given by:

$$\theta_{Li} = \cos^{-1}\left(\frac{T_{w0}}{T_s}\right) \tag{4}$$

This relationship was verified by performing a number of shear tests using a parallelogram fixture and measuring the change in tow width using a digital camera. The results agreed extremely well with the predicted values.

Prior to lateral contact (ie. when $\theta \le \theta_{Li}$), the tow contact force arises from the pre-tension within the fabric. Once the tows come into contact an additional force arises from inter-tow compaction. In this model the compaction model developed by Cai and Gutowski [9] for aligned fibre bundles is used. The fibre bundle stress can be obtained from:

$$\sigma_b = \frac{e_b \cdot F_{11}}{\left(F_{bb} \cdot F_{11} - F_{b1}^2\right)} \tag{5}$$

where e_b is the bundle strain and F_{11}, F_{bb} and F_{b1} are compliance terms, which are functions of the fibre modulus and instantaneous fibre volume fraction of the bundle. The fibre bundle stress is integrated over the tow contact area and substituted into Eqn. 1 to obtain the torque at a tow crossover. The shear force is then calculated from the sum of the torque contributions for each crossover.

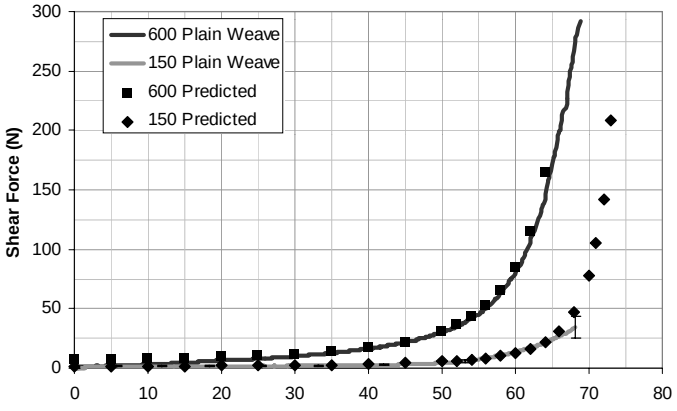

Typical predictions appear in Fig. 6 for two plain weave fabrics, using the parameters given in Table 1. The experimental results were obtained using a parallelogram shearing fixture mounted in a mechanical testing machine. Each test was carried out at 100mm/min. As shown in the figure, the predictions are in good agreement with the experimental results. However it should be noted that not all of the variables in Table 1 could be measured directly. Both the fabric pre-tension and thickness were chosen to obtain reasonable agreement with the experimental results. To obtain consistent results, pre-tension is applied to the fabric using a clamping frame prior to mounting within

the shearing fixture. However, it is thought that some degree of relaxation occurs prior to testing. This problem should be eliminated by improving the experimental procedure. The fabric thickness may be determined once a suitable model for the deformation of an individual tow has been developed.

Table 1: Fabric data for mechanical fabric shear model

	600 g/m^2 plain weave	150 g/m^2 plain weave
Tow width (mm)	3.1	1.2
Tow spacing (mm)	4.0	2.0
Linear density (Tex)	1190	150
Thickness (mm)	2	0.6
Pre-Tension (N)	100	50

Despite the above reservations, the model produces encouraging results. In particular, it seems capable of anticipating the rapid increase in shear force which occurs immediately prior to fabric wrinkling (indicative of the locking angle). The model is presently being developed to predict the shearing behaviour of other textile architectures.

ENERGY APPROACH TO DEFORMATION MODELLING

The conventional approach to drape simulation for reinforcement fabrics is to model the material as a pin-jointed net. A unique draped pattern can be obtained by specifying two intersecting fibre paths, referred to as generators, on the surface of the preforming tool, from which the remaining fibres can be positioned using a geometric mapping. This approach works well for symmetric shapes draped with balanced fabrics, but is less satisfactory for non-symmetric shapes or for fabrics which have a preferential direction for shearing. This is demonstrated in Fig. 7, which shows the fibre patterns for hemispherical preforms produced using two warp-knitted fabrics from Tech Textiles. Samples were produced using matched tooling mounted in a mechanical testing machine, with fibres marked prior to forming to illustrate the subsequent deformation. Despite the component symmetry, two very different non-symmetric fibre patterns were obtained. Both fabrics were restricted in quadrants sheared parallel to the stitching thread, with the effect most pronounced for the chain stitch.

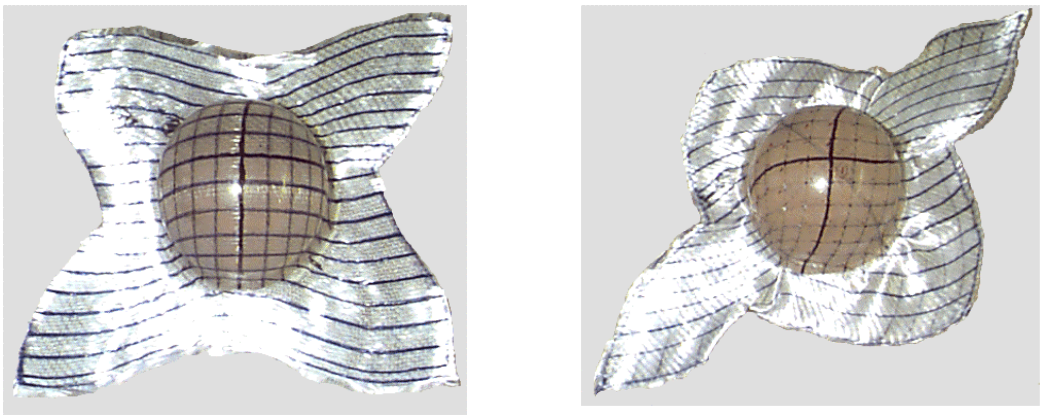

Fig. 7: Hemispherical preforms produced using ±45^o warp-knitted fabrics – left: E-BXhd 936 (tricot 1 and 1 stitch), right: E-BX 318 (chain stitch).

A more sophisticated approach to fabric deformation modelling involves a sequential simulation using the finite element method. This can overcome some of the above problems at the expense of increased computation time. An alternative approach is therefore proposed,

utilising the existing pin-jointed mapping within an iterative scheme. The strain energy required to produce each mapping will be calculated, with the mapping resulting in the lowest energy assumed represent the behaviour of the fabric.

The total strain energy would consist of several components, including contributions from inter-tow shear and slippage, tow straightening (for woven fabrics), ply/tool and ply/ply friction. It is proposed to base the model initially on the contribution from inter-tow shearing alone, as this is thought to be most indicative of the effect of fabric construction on deformation. Fig. 8 shows the shear force curves for the two warp-knitted fabrics mentioned above, sheared both parallel (stitch tension) and perpendicular (stitch compression) to the stitching thread. Both curves exhibit substantially higher shear forces for deformation parallel to the stitch, with the effect most pronounced for the fabric retained using a chain stitch (E-BX 318). The curve for this material reaches a peak at around 35^o shear, which corresponds to failure of the stitching thread. After this point, the shear force reduces significantly until inter-tow compaction leads to a second increase in force.

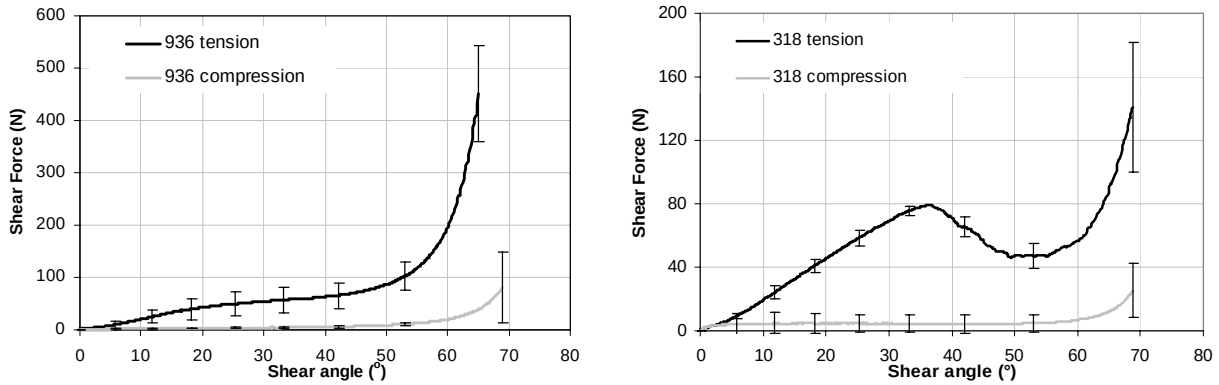

Fig. 8: Shear force curves for E-BXhd 936 (left) and E-BX 318(right).

The shear strain energy can be calculated simply by considering the area under the torque-shear angle curve [10]:

$$U_s(\theta) = \int_0^{\theta} T(\gamma) d\gamma \qquad [6]$$

where $T(\gamma)$ is the torque required to achieve a shear angle γ. This is demonstrated in Fig. 9 for the shear data from Fig. 8. For convenience, a polynomial was fitted to the shear force data to allow the integration to be carried out, although ultimately the mechanical shear model would be used to calculate the forces. The curves in Fig. 9 represent shear strain energy per unit area, from which the total shear strain energy can be calculated for an arbitrary fabric sample size. This can be achieved within the fabric drape simulation by simply summing the contribution at each node.

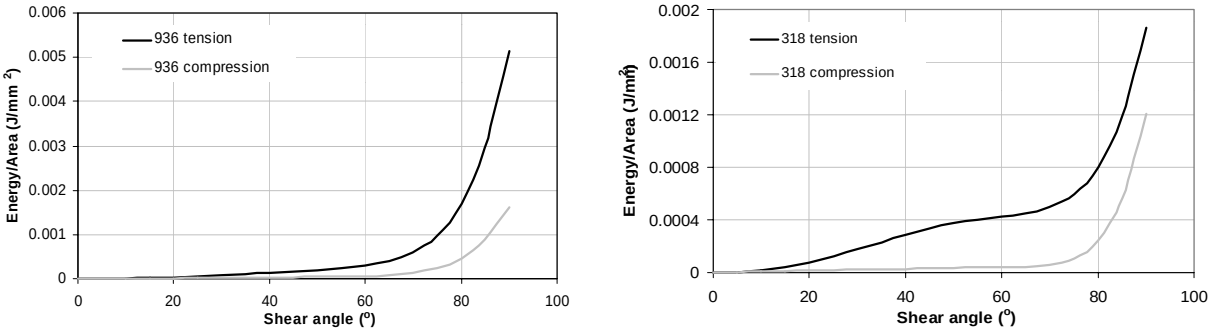

Fig. 9: Shear strain energy curves for E-BXhd 936 (left) and E-BX 318(right).

A simple way to determine the mapping resulting in the minimum energy is to develop an iterative scheme based on the two generator fibre paths. The approach would then involve simply finding the two intersecting paths which resulted in the lowest energy mapping. From the experimental results shown in Fig. 7, one possible approach for the hemispherical mould would be to simply vary the angle of intersection of these fibres. Fig. 10 shows a graph of total shear strain energy against this intersection angle. It is clear that an optimum value exists for both fabrics (approximately 75^{o} for E-BXhd 936 and 60^{o} for E-BX 318). Fig. 11 shows the predicted fibre pattern for each fabric using these angles. Comparison with Fig. 7 shows that the predicted optimum mappings correspond reasonably well with the experimental results. Clearly there is some room for improvement, as the actual fibre paths which correspond to the generator fibres (marked as bold lines on Fig. 7) are curved rather than straight. Nevertheless this approach appears to show some potential. The next stage will be to develop a more sophisticated iterative scheme which will allow the initial paths to be determined more accurately. The model will then be tested for a wide range of fabrics and for more challenging, non-symmetric geometries.

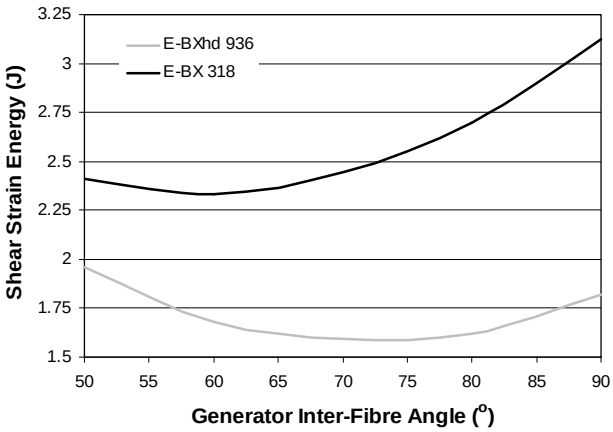

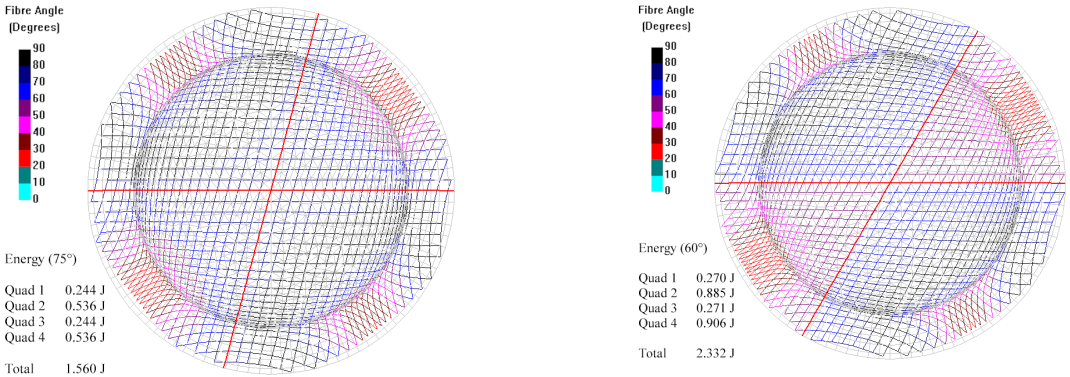

Fig. 11: Comparison of deformed fibre patterns – optimum for E-BXhd 936 (left), optimum for E-BXhd 318 (right).

CONCLUSIONS

It is clear from the experimental results presented in this paper that fibre architecture can have a significant effect on the deformation characteristics of a fabric. This has been shown even for a simple axi-symmetric geometry, where significantly different results were obtained for preforms produced using two similar warp-knitted fabrics. Shearing tests indicate that this is related to the difference in the forces required to shear the material parallel and perpendicular to the stitching thread. To attempt to account for this, a geometric model for woven and warp-knitted fabrics has been developed as a basis for a mechanical model for fabric shearing behaviour. The mechanical model allows shear forces to be predicted based on inter-tow friction and tow compaction, and appears able to represent the behaviour of plain woven fabrics very accurately. This is being used to develop an enhanced draping simulation, which utilises the conventional kinematic mapping within an iterative scheme to determine the fibre pattern which results in the minimum strain energy. Preliminary results are promising, suggesting that this may lead to a more accurate draping simulation with the capability to account for the effects of fabric construction on forming characteristics.

ACKNOWLEDGEMENTS

The authors would like to thank the following organisations for their continued support: The Engineering & Physical Sciences Research Council, Ford Motor Company, Rolls Royce, Dowty Aerospace Propellers, Flemmings Industrial Fabrics, Brookhouse Patterns.

REFERENCES

1. Yu, J., Cai, Z., & Ko, F.K. "Formability of textile preforms for composites applications – Part 1: characterisation experiments", *Composites Manufacturing* Vol. 5, 1994, pp. 113-121.
2. Long, A.C., Rudd, C.D., Blagdon, M. & Johnson, M.S. "Experimental analysis of fabric deformation mechanisms during preform manufacture", *Proc. 11th Int. Conf. on Composite Materials*, Gold Coast, Queensland, Australia, July 1997, Vol V, pp. 238-248.
3. McBride, T.M. "The large deformation behaviour of woven fabric and microstructural evolution in formed textile composites", PhD Thesis, Boston University, 1997.
4. Van West, B.P., Pipes, R.B. & Keefe, M. "A simulation of the draping of bidirectional fabrics over arbitrary surfaces", *J. Textile Institute* Vol. 81, 1990, pp. 448-460.
5. Long, A.C. & Rudd, C.D. "A simulation of reinforcement deformation during the production of preforms for liquid moulding processes", *IMechE J. of Engineering Manufacture* Vol. 208, 1994, pp. 269-278.
6. Boisse, P., Borr, M., Buet, K. & Cherouat, A. "Finite element simulations of textile composite forming including the biaxial fabric behaviour", *Composites Part B* Vol. 28, 1997, pp. 453-464.
7. de Luca, P., Lefébure, P., Pickett, A.K., Vodermayer, A.M. & Werner, W. "The numerical simulation of press forming of continuous fiber reinforced thermoplastic prepregs", *Proc. 28th Int. SAMPE Technical Conf.*, Nov 1996, Seattle, USA.
8. Kawabata, S. Niwa, M. & Kawai, H. "The finite deformation theory of plain-weave fabrics", *J. Textile Institute* Vol. 64, 1973, pp. 21-85.
9. Cai, Z. & Gutowski, T. "The 3D deformation behaviour of a lubricated fibre bundle", *J. Composite Materials* Vol. 26, 1992, pp. 1207-1237.
10. Ye, L. & Daghyani, H.R. "Characterisation of woven fabric reinforced composites in forming process", *Composites Part A*, Vol. 28, 1997, pp. 869-874.